

# Raman scattering and x-ray diffraction characterization of amorphous semiconductor multilayer interfaces

D. D. Allred, J. Gonzalez-Hernandez, O. V. Nguyen, D. Martin, and D. Pawlik  
*Energy Conversion Devices, Inc., 1675 West Maple Road, Troy, Michigan 48084*

(Received 23 January 1986; accepted 2 May 1986)

Raman spectroscopy (RS) and low-angle x-ray diffraction (LAXRD) have been used to characterize semiconductor multilayer interfaces. In the present study a model for Raman spectra of multilayers is developed and applied to the specific case of the interfaces of *a*-Si/*a*-Ge multilayers. Quantification of the "blurring" of interfaces is possible because peak heights in the Raman spectra of thin films are proportional to the number of scatterers, thus RS is capable of directly "counting" the total number of chemical bonds of a given type in the film. Multilayers, prepared by various deposition techniques, are compared. The relative roles of LAXRD and RS in investigating interfaces are contrasted. Several *a*-Si/*a*-Ge multilayers deposited by ultra-high vacuum (UHV) evaporation (MBD) are found to exhibit very regular periodicities and exceptionally sharp interfaces ( $< 1.0 \text{ \AA}$  intermixing).

## I. INTRODUCTION

Recent developments in thin film technology have made it possible to prepare and characterize very regular, periodic, multilayered thin film structures. This has created a great deal of interest, both on a basic and technological level. Several groups<sup>1,2</sup> have prepared periodic structures composed of alternating layers of tetrahedrally bonded amorphous semiconductors and insulators. It has been stated that the optical and electrical properties of those amorphous multilayers suggest quantum size effects similar to those observed in crystalline<sup>2</sup> superlattices. In addition, periodic multilayers consisting of alternating thin layers (from 10–100 Å) of high-density and low-density materials have been shown to act as efficient Bragg diffractors for x rays.<sup>3,4</sup>

Characterizing thin film multilayers containing layers that may be only a few atoms thick has required the development of specialized techniques. Progress has proceeded one step at a time. Many prior structural studies sought to establish the existence of regular layering in multilayers and to determine the layer spacing.<sup>2,4</sup> Others sought to observe atom-to-atom bonding changes that may occur when atoms are constrained in ultra-thin films.<sup>1,5</sup> Quite recently attention has shifted to the interfaces between layers, first using low-angle x-ray diffraction (LAXRD)<sup>3</sup> and then using Raman spectroscopy (RS).<sup>6,7</sup> RS has been shown to be a valuable tool for characterizing the interfaces of *a*-Si/*a*-Ge alloy multilayers.

In the present study we focus on the use of Raman spectroscopy (RS) for characterizing semiconductor multilayer interfaces. In particular we present a model for the analysis of the Raman spectra of semiconductor periodic multilayers and discuss the specific case of *a*-Si and *a*-Ge multilayers.

The model finds application in distinguishing the interfacial sharpness of multilayer films prepared by a spectrum of deposition techniques including ultra-high vacuum evaporation, also called molecular beam deposition (MBD), ion beam and magnetron sputtering, and glow discharge. This study, which was first summarized in Ref. 7, marks the first report of the use of MBD and magnetron sputtering for the preparation of amorphous semiconductor multilayers. Of the films studied, several MBD-multilayers exhibited the sharpest interfaces ( $< 1.0 \text{ \AA}$ ). The role of substrate heating and the suitability of other deposition techniques in achieving sharp interfaces is also addressed.

The interfacial roughness parameter determined by low-angle x-ray diffraction (LAXRD), a long known technique for characterizing interfacial sharpness in multilayers, is in good agreement with Raman.

## II. EXPERIMENTAL

### A. Preparation

Amorphous multilayer structures were prepared by a number of techniques. With the exception of those prepared by rf glow discharge process, all films were silicon germanium multilayers. The thickness of the silicon and germanium layers in each period were generally as close to equal as possible. In each of these cases, among the samples prepared were those with an approximately 100 Å period, Si/Ge (50 Å/50 Å). Fused quartz, 7059 glass, and silicon (100) test wafers were employed as substrates. The deposition techniques utilized included the following.

(1) Evaporation in ultra-high vacuum (MBD): A PHI-400 MBD system, with a base pressure in the low  $10^{-10}$  Torr scale, was employed to deposit multilayers

composed of unhydrogenated *a*-Si layers alternating with layers of unhydrogenated *a*-Ge (*a*-Si/*a*-Ge). The multilayers were produced by subsequential electron evaporation from pure silicon and germanium sources. Precise layering was achieved using pneumatic shutters in front of the sources. The shutters were controlled by a Sloan thickness monitor. The deposition rate set at 1 Å/s for both materials. The thickness of individual layers ranged from 10–200 Å and in most multilayers 25 layer pairs were deposited.

(2) Ion beam sputtering: An Ar ion beam from a 2.5 cm Kaufman ion source, operating in pure Ar, was caused to strike alternately one or another target. The targets were attached to a disk mounted on a pivot and could be automatically and reproducibly rotated into the path of the ion beam. The ion beam was shut off while the targets were rotated. To promote uniformity the samples were also rotated during deposition. In the preparation of Si/Ge multilayers, the targets were > 5N Si (cast) and 6N Ge (hot pressed). The substrate was heated by radiation. The thickness of the individual layers was nominally 5 nm. A detailed description of an ion beam sputtering system can be found elsewhere.<sup>8</sup>

(3) Magnetron sputtering: A Sloan model SL 1800 four-target, horizontal magnetron sputtering system was used to prepare Si/Ge multilayers via rf sputtering. Layering is achieved by rotating the carousel on which the samples were mounted. The rotation speed was chosen to control layer thickness, whereas the ratio of Si to Ge thickness was fixed by adjusting each target's power. The plasma above each target remained lit while the substrates rotated. To minimize intermixing, the silicon and germanium targets were separated by one or more unused target locations. The instantaneous sputtering rate for Si and for Ge was 14–18 Å/s. Periodicities ranged from 8–100 Å.

(4) Alternating layers of *a*-Si:H/*a*-SiN:H were grown by an rf glow discharge following a method described elsewhere.<sup>9</sup>

## B. Characterization

X-ray diffraction (XRD), which employed a Philips XRD-2500 x-ray diffractometer, was the nonoptical method chosen to obtain structural data. Special attention was given to low-angle diffraction (LAXRD). The presence of regular periodicity and the dimensions are the data immediately accessible from LAXRD. Filtered Cu and Cr  $K_{\alpha}$  lines were employed, but Cr was preferable for low-angle measurements. Multiplying the period thicknesses by the number of periods is potentially the most accurate technique for measuring the thickness of the multilayers. Thickness data were also obtained using a mechanical stylus technique. Details on measurements of film absorptance ( $\alpha$ ) and refractive index can be found elsewhere.<sup>10</sup>

The LAXRD data contain information of interfacial roughness. The model proposed by Underwood *et al.*<sup>4</sup> for the diffraction behavior of a layered synthetic multilayer has been used in the work. The thickness of the interfacial roughness, as deduced by that model, was obtained from the integrated intensity under the low-angle XRD peaks. Abeles *et al.*<sup>2</sup> have already applied the model to determine the roughness parameter in *a*-Si:H/*a*-SiN<sub>x</sub>:H multilayers.

The film average compositions and impurity content were determined by Auger electron spectroscopy (AES) and electron spectroscopy for chemical analysis (ESCA). The IR transmission data were also examined for the presence of O, N, H, and C modes. Certain thick films were examined by electron microprobe microanalysis. The instrument employed was a JEOL (model SM-35C) with a Kevex model Unispec 7077 solid-state detector for energy dispersive x-ray (EDX) analyses. Kevex software, Magic V, was employed for data analysis. The energy of the exciting electron beam was set high enough for the multilayer to appear homogeneous, but low enough that substrate atoms were not analyzed. This provided a check on other methods for determining the relative thickness of the layers.

The 514.5 nm line from a Spectra Physics model-8 W Ar ion laser was used for the Raman studies. A Spex double grating spectrometer provided spectral analysis of the Raman scattered light. A standard photon counting system was employed for detection and analysis. In the next section we consider the use of RS to study multilayer interfaces.

## III. INTERPRETATION OF DATA

### A. Modeling the Raman spectrum of a multilayer

Raman spectroscopy has been shown to be a very useful technique to characterize the structure of single layers of amorphous semiconductors.<sup>11</sup> Previous publications of the uses of RS to characterize multilayer structures have employed its sensitivity to observed quantitative changes in the microscopic structural order of thin layers, particularly the bond-angle distribution width.<sup>1,5</sup> Recently it has been reported that RS can detect Si-Ge bonds at interfaces in *a*-Si/*a*-Ge multilayers.<sup>6,7</sup>

The purpose of this section is to develop a method for employing RS data for quantitatively determining intermixing at interfaces in multilayers.

Quantification of the blurring of interfaces is possible because peak heights in the Raman spectra of thin films are proportional to the number of scatterers, thus RS is capable of directly "counting" the total number of chemical bonds of a given type in a thin film. This is particularly true in amorphous material since the

phonon decay length is on the order of the lattice constant. Thus each site acts like a single scatterer.

The development in Sec. III B is valid if the following conditions prevail.

- (1) It is known that the material is layered.
- (2) Changes in the composition of materials should produce significant changes in the RS spectrum. The spectrum of the alloy produced by intermixing should be significantly different than either of the parent materials over at least a portion of its spectrum.

(3) The absorptance at the RS wavelength chosen, of each of the layers in the multilayers and the products of their intermixing, is large enough for the Raman cross section to be significant but small enough that the beam is not totally attenuated before it reaches the next interface. For periodicities of approximately 100 Å,  $\alpha$  should be greater than  $10^4 \text{ cm}^{-1}$  and less than  $10^6 \text{ cm}^{-1}$ .

(4) Thin film optical interference effects can be neglected so that exponential decay describes the absorptance of light in each layer. Optical interference occurs when a traveling electromagnetic wave encountering changes in index. In multilayers interference effects can occur, on the one hand, between individual layers of the multilayer film and, on the other hand, between the air-film and film-substrate interfaces. The first effect—interference between individual layers in a periodic multilayer—is negligible if the reflectance amplitude ( $r$ ) between layers is small or if the distance ( $d$ ) between interfaces is much smaller than the wavelength of light in the medium. The second source of interference can also be handled without difficulty. To simplify the following analysis it is assumed that the multilayer is sufficiently absorbing that the laser light will be substantially attenuated before it strikes the back interface.

### B. Development of the model

Let us consider a multilayer structure consisting of Z periodic layer, as shown in Fig. 1. The top layer of the total structure is layer A. The effective thickness and the absorption coefficient at the Raman wavelength ( $\lambda_R$ ) of each individual layer A, B, ..., Z are denoted by  $l_A$ ,  $l_B$ , ...,  $l_Z$ , and  $\alpha_A$ ,  $\alpha_B$ , ...,  $\alpha_Z$ , respectively.

The symbols  $\ell_A$ ,  $\ell_B$ , ...,  $\ell_Z$  denote the actual path lengths the light travels when the multilayer is illuminated at an off-normal angle.

Employing these definitions, the total intensity of Raman scattered light from all layers A in the structure  $I_A$  can be written as

$$I_A = I'_A (1 + S^2 + S^4 + S^6 + \dots) = I'_A / (1 - S^2), \quad (1)$$

where  $I'_A$  and  $S$  are defined by

$$I'_A = (I_0 \Sigma_A / 2\alpha_A) [1 - \exp(-2\alpha_A \ell_A)] \quad (2)$$

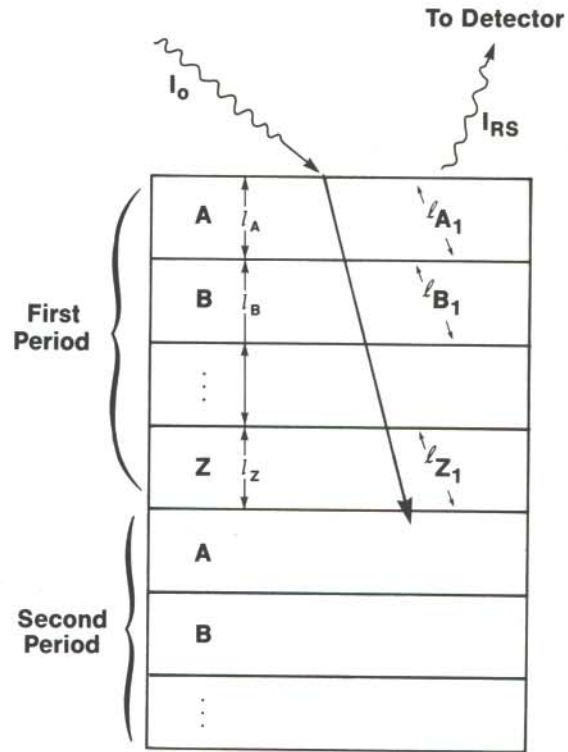


FIG. 1. Schematic representation of a Z layer periodic multilayer structure.  $\ell_A$ ,  $\ell_B$ ,  $\ell_Z$ , and  $\alpha_A$ ,  $\alpha_B$ ,  $\alpha_Z$  are the path length of light and absorption coefficient for layer A, C, and Z, respectively.

and

$$S = \exp[-(\alpha_A \ell_A + \alpha_B \ell_B + \dots + \alpha_Z \ell_Z)] \quad (3)$$

Here  $I'_A$  is the intensity of Raman scattering due to the top A layer alone and  $I_0$  is the intensity of the laser beam entering the structure. When the Brewster angle geometry is chosen, reflectance losses are minimized and, to a good approximation,  $I_0$  is also the intensity of the laser beam external to the multilayer. The Raman cross section of material A is  $\Sigma_A$ .

Substituting  $I'_A$  and  $S$  in Eq. (1) we have

$$I_A = I_0 \Sigma_A [1 - \exp(-2\alpha_A \ell_A)] / [2\alpha_A (1 - S^2)] \quad (4)$$

Similarly, the added Raman intensity from layers B...X is given by

$$I_B = \frac{I_0 \Sigma_B \exp(-2\alpha_A \ell_A) [1 - \exp(-2\alpha_B \ell_B)]}{[2\alpha_B (1 - S^2)]}, \quad (5)$$

$$I_X = (I_0 \Sigma_X / 2\alpha_X) \exp[-2(\alpha_A \ell_A + \dots + \alpha_{X-1} \ell_{X-1})] \times [1 - \exp(-2\alpha_X \ell_X)] \times \{1 - \exp[-2(\alpha_A \ell_A + \dots + \alpha_Z \ell_Z)]\}^{-1}, \quad (6)$$

where  $\Sigma_B$  and  $\Sigma_X$  are the Raman cross sections for material B and X, respectively.

We will consider the specific case of a biperiodic multilayer structure consisting of layer pairs A and C separated by interfacial layers B and B' as pictured in Fig. 2. We further make the assumption that the interface produced by depositing A on C is the same as depositing C on A, that is,  $B = B'$ , while  $l_A$  ( $l_C$ ) is the actual thickness of the A (C) layer after intermixing.  $I_B$  stands for the intensity from both layers. From Eqs. (4) and (5), the intensity ratio  $I_B/I_A$  is expressed as

$$\frac{I_B}{I_A} = \frac{2\alpha_A \Sigma_B l_B [1 + \exp(-2\alpha_C l_C)]}{\Sigma_A [\exp(2\alpha_A l_A) - 1]}, \quad (7)$$

where we have made the assumption that  $l_B \ll l_A$ . From Eq. (7) the quantity  $l_B$  can be expressed as

$$l_B = \frac{[\exp(2\alpha_A l_A) - 1]}{2\alpha_A [1 + \exp(-2\alpha_C l_C)]} \frac{I_B \Gamma_{AB}}{I_A}, \quad (8)$$

where  $\Gamma_{AB} = \Sigma_A / \Sigma_B$ .

Following the derivation of (8),  $l_B$  can be alternatively calculated in terms of  $I_B/I_C$ :

$$l_B = \frac{[1 - \exp(-2\alpha_C l_C)]}{2\alpha_C [1 + \exp(-2\alpha_C l_C)]} \frac{I_B \Gamma_{CB}}{I_C}, \quad (9)$$

where  $\Gamma_{CB} = \Sigma_C / \Sigma_B$ .

Standard samples, one of composition A or C and the other of composition B, must be measured under identical experimental conditions. All samples need to be thicker than the penetration length of the laser light used for the Raman measurements. The measured Ra-

man intensities from the standard samples are termed  $I_A$ ,  $I_C$ , and  $I_B$ , respectively. The Raman intensity  $I$  is  $\Sigma V$ , with  $V$  being the scattering volume. Since  $V$  is proportional to  $1/\alpha$ , the ratio  $\Gamma_{XY}$  may be expressed by  $\Gamma_{XY} = I_X \alpha_X / I_Y \alpha_Y$ , in which  $\alpha_Y$  and  $\alpha_X$  are the measured absorption coefficients of standard samples Y and X.

It is usually observed that as long as the total number of X-X bonds in sample X are not diluted by alloying or the presence of voids,  $\Sigma_X$  will be reasonably constant even though preparation conditions might vary.<sup>12</sup> It is often possible, therefore, to employ one value of  $\Sigma$  for samples deposited under a variety of deposition conditions.

In contrast with  $\Sigma$ , which is relatively invariant, it is well known that  $\alpha$  for amorphous semiconductors near their absorption edges can depend strongly on preparation conditions. It is important, therefore, to note that neither Eqs. (8) nor (9) depend on  $\alpha_A$  or  $\alpha_C$  to first order if  $\alpha_A l_A$  or  $\alpha_C l_C$  are small. Expanding exponentials (8) and (9) become, respectively,

$$l_B = \frac{l_A [1 + \alpha_A l_A + \Theta^{(2)}] I_B \Gamma_{AB}}{\{I_A [1 + \exp(-2\alpha_C l_C)]\}}, \quad (10)$$

$$l_B = l_C [1 - (\alpha_C l_C)^2/3 + \Theta^{(3)}] I_B \Gamma_{CB} / I_C, \quad (11)$$

where  $\Theta^{(n)}$  means terms of order  $n$  or higher in  $\alpha l$ .

When  $\alpha l$  is small, it is, therefore, not necessary to measure  $\alpha$  for each combination of preparation technique and conditions. This is an important savings. Equations (10) and (11) explicitly confirm intuition that  $l_B$  is equal to  $l_A$  or  $l_C$  weighted by the ratios of the appropriate cross sections and peak intensities. It is also worthy to note that the first-order term in  $\alpha_C l_C$ , inside the square brackets in Eq. (11), is identically zero.

All of the above analysis is correct for both integral and differential (wavenumber by wavenumber) quantities; integral data (total scattering under a given peak) are generally preferable since integrating a spectrum diminishes the effect of noise.

### C. Application of the model to silicon-germanium multilayers

In the past few years, Raman scattering has been extensively used to analyze the structure of single layers of *a*-Si, *a*-Ge and their alloys.<sup>11</sup> In tetrahedrally bonded amorphous semiconductors, due to the breakdown of momentum conservation, all phonons in the crystalline phonon dispersion curve are allowed; therefore, the Raman spectrum resembles the broadened crystalline density of states (DOS). As shown in Fig. 3(a), the Raman spectrum of an *a*-Si(*a*-Ge) thin film shows two prominent humps located around 140 (75) and 480  $\text{cm}^{-1}$

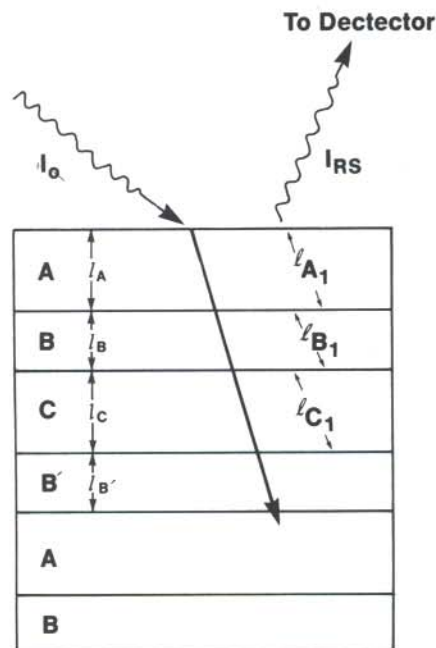


FIG. 2. Schematic representation of a biperiodic multilayer structure with intermix regions B and B'.  $l_A$ ,  $l_B$ ,  $l_C$ , and  $l_{B'}$ , and  $l_A$ ,  $l_B$ ,  $l_C$ , and  $l_{B'}$  are the path lengths of light in and the thicknesses of layers A, B, C, and B', respectively. It is assumed  $B = B'$ .

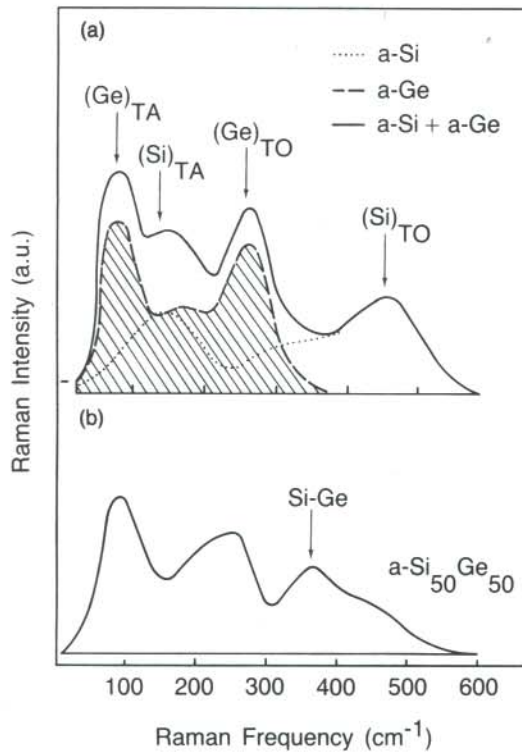


FIG. 3. (a) Typical Raman spectra for an amorphous germanium film (dashed), amorphous silicon film (dotted), and the sum of both (continuous). The origin of the Raman peaks are noted above the curves. (b) A typical Raman spectrum for an  $a\text{-Si}_{0.5}\text{Ge}_{0.5}$  alloy. The arrow above  $380\text{ cm}^{-1}$  indicates the position of the Si-Ge local vibrational modes.

( $270\text{ cm}^{-1}$ ). The former has its origins in the transverse acoustic (TA) phonons while the latter is related to the transverse optical (TO) phonons.<sup>13</sup> The continuous curve in the top part of Fig. 3(a) represents the sum of  $a\text{-Si}$  and  $a\text{-Ge}$  Raman spectra.

The Raman vibrational properties of random  $a\text{-Si}_x\text{Ge}_{1-x}$  alloys can also be correlated to the DOS of their crystalline counterparts.<sup>14</sup> Figure 3(b) shows a typical Raman spectrum for an  $a\text{-Si}_{0.5}\text{Ge}_{0.5}$  alloy. The spectrum exhibits features common to both  $a\text{-Si}$  and  $a\text{-Ge}$  that arise from vibrations associated with Si-Si and Ge-Ge pairs, respectively. In addition, a peak that is not present in either the pure  $a\text{-Si}$  or  $a\text{-Ge}$  is observed at approximately  $380\text{ cm}^{-1}$ . The position of this peak shifts as the composition of the  $a\text{-Si}_{1-x}\text{Ge}_x$  changes. Its relative strength is also a measurement of the chemical composition in the alloy and is proportional to  $x(1-x)$  for  $a\text{-Si}_{1-x}\text{Ge}_x$  alloys. Its presence fulfills requirement (2) above.

The other conditions stated in the development of the model dictate that multilayer samples having periodicities less than or equal to about  $200\text{ \AA}$  and containing an  $a\text{-Ge}$  total thickness greater than  $500\text{ \AA}$  are most susceptible to analysis. The requirement that the laser

probes at least one germanium layer (two interfaces), restricts the germanium thickness in each layer to  $200\text{ \AA}$ , while the restriction that the beam be substantially attenuated at the back of the thin film dictates that the total thickness of germanium be at least  $500\text{ \AA}$  to limit the reflectance at a glass interface to less than 1%. Since  $a\text{-Ge}$  is several times more absorbing than  $a\text{-Si}$  ( $5 \times 10^5\text{ cm}^{-1}$  vs  $2 \times 10^5\text{ cm}^{-1}$ ), the thickness of  $a\text{-Si}$  is not generally an issue.

The requirement that interference effects between layers are negligible needs more careful attention. Consider a thin film of thickness  $d$  and with refractive indices  $n_1$  and  $k_1$  sandwiched between two slabs of a second material ( $n_2, k_2$ ). In the limit of zero absorptance in the film, the magnitude of the composite reflectance amplitude  $r_{\text{comp}}$  from the two surfaces of the first material at wavelength  $\lambda$  is

$$|r_{\text{comp}}| = \frac{|r| [1 - \exp(-2i\delta)]}{[1 - r^2 \exp(-2i\delta)]}$$

Where the phase change  $\delta = 2\pi nd/\lambda$  and  $|r|$  is the magnitude reflectance amplitude from either of the surfaces,

$$|r| = \{[(n_1 - n_2)^2 + (k_1 - k_2)^2] [(n_1 + n_2)^2 + (k_1 + k_2)^2]^{-1}\}^{1/2}$$

Neglecting  $r^2 \exp(-2i\delta)$ ,

$$|r_{\text{comp}}| = 2|r| \sin \delta$$

When  $\delta$  is small,

$$|r_{\text{comp}}| = 4\pi|r|nd/\lambda;$$

$|r_{\text{comp}}|$  becomes negligible when  $|r|$  and/or  $nd/\lambda$  are small.

For  $a\text{-Si}$  ( $a\text{-Ge}$ ), we use as  $n$  and  $k$ , 4.7 and 0.8 (4.9 and 2.0) at  $514\text{ nm}$ .<sup>15</sup> For  $5.0\text{ nm}$  thick Si layers,  $\delta = 0.25$  radians and  $|r_{\text{comp}}| = 0.1$ . Since reflectance intensity is proportional to  $r^2$ , it can be concluded that the effect on the reflected intensity is less than 1% per period for  $100\text{ \AA}$  periods. Even for thick layers where  $\delta$  reaches  $\pi/2$  radians, the maximum value  $|r_{\text{comp}}|^2$  is 0.04. The actual effect in the multilayers will be much smaller due to partial cancellation from neighboring layer pairs.

In our work, as is common for RS, the Brewster angle is chosen to minimize specularly reflected light. For this geometry

$$\ell_i = l_i [1 + (n_0/n_i)^2]^{1/2}, \quad i = \text{A, B, C, etc.},$$

where  $n_0$  is 1.0 for air and  $n_i$  is the refractive index of the semiconductor. For high-index semiconductors, the relative difference between the  $\ell_i$  and  $l_i$  is  $\frac{1}{2}(n_i)^{-2}$ . This is less than 3% for silicon and germanium alloys. In  $a\text{-Si}/a\text{-Ge}$  multilayers, therefore, the difference between  $l_i$  and  $\ell_i$  is negligible.

#### IV. RESULTS AND DISCUSSION

In order to demonstrate the use of RS to investigate the structure of interfaces, the model described in Sec. III was applied to *a*-Si/*a*-Ge multilayers. In all the *a*-Si/*a*-Ge samples studied, the last layer deposited was silicon. Thus the layers A, B, and C in Fig. 2 stand for *a*-Si, an *a*-Si<sub>1-x</sub>Ge<sub>x</sub> alloy and *a*-Ge, respectively.

In Fig. 4, the Raman spectra for three *a*-Si/*a*-Ge multilayers prepared by MBD ( $T_s = 300^\circ\text{C}$ ), ion beam ( $T_s = 275^\circ\text{C}$ ) and magnetron sputtering ( $T_s = 25^\circ\text{C}$ ) are compared. Each spectrum has been decomposed significantly into three components: *a*-Si (dashed line), *a*-Ge (dotted line), and *a*-Si<sub>1-x</sub>Ge<sub>x</sub> (continuous line). These added together give the best fit to the measured integrated Raman intensity. The position of the Si<sub>1-x</sub>Ge<sub>x</sub> peak ( $380\text{ cm}^{-1}$ ) in all cases corresponds most closely to Si<sub>0.5</sub>Ge<sub>0.5</sub>. This, then, fixes the composition of layer B. Notice that a much-reduced *a*-Si<sub>0.5</sub>Ge<sub>0.5</sub> component is observed for the MBD sample. Using Eq. (8) the interfacial layer thickness  $l_B$  has been determined from the integrated Raman intensities under the

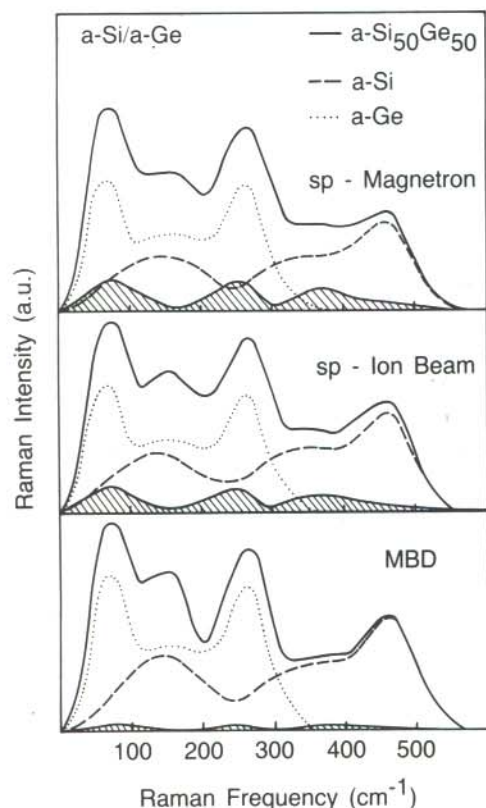


FIG. 4. Raman spectra for *a*-Si/*a*-Ge multilayers prepared by magnetron sputtering (top), ion beam sputtering (middle), and MBD (bottom). These samples correspond to the sixth, fifth, and third entries in Table I, respectively. Each spectrum has been decomposed into three components, *a*-Si (dashed), *a*-Ge (dotted), and *a*-Si<sub>1-x</sub>Ge<sub>x</sub> (continuous). In all cases  $x \approx 0.5$  was found.

*a*-Si<sub>0.5</sub>Ge<sub>0.5</sub> and *a*-Si curves. We find that  $l_B$  is 3.1, 5.3, and  $6.2\text{ \AA}$  for these MBD, ion beam, and magnetron sputtered samples, respectively.

The interfacial layer thickness  $l_B$  contains two components: the number of bonds that an atomically smooth surface would have with the layer above it, and any arising from intermixing. The model developed above is macroscopic and mathematically combines these bonds together. Thus  $l_B$  is larger than the true intermixed layer thickness. To properly calculate intermixing requires a proper accounting of the density of bonds at a growing *a*-Si or Ge film. This quantity can be estimated, based on the fact that for the growth of polycrystalline tetrahedral semiconductors on an amorphous substrate at the lowest temperature where partial crystallization begins, the (110) and (111) orientations are approximately equally preferred and dominate.<sup>16</sup> The (100) orientation is absent. The bond density for the (111) and (110) surfaces of Si<sub>0.5</sub>Ge<sub>0.5</sub> are calculated to be  $11.3$  and  $9.2 \times 10^{14}\text{ cm}^{-2}$ .<sup>17</sup> The bond density of the amorphous structure just below this temperature might be expected to be similar to the average of the (111) and (110) surfaces, about  $10.3 \times 10^{14}\text{ cm}^{-2}$ . This is equivalent to  $2.2\text{ \AA}$  of Si<sub>0.5</sub>Ge<sub>0.5</sub>. The intermixing width  $w$  for the samples is then 1.0, 3.0, and  $4\text{ \AA}$ , respectively, for these MBD, ion-beam, and magnetron sputter samples. These numbers are summarized in Table I.

From the LAXRD data, values of the interfacial roughness ( $\xi$ ) and the thickness ratio of the top layer to the period of the multilayer ( $\eta$ ) were calculated using the technique of Underwood.<sup>4</sup> Table I contains the periodicity ( $p$ ) from LAXRD, ( $\xi$ ), ( $\eta$ ), the number of diffraction orders observed ( $m$ ), and the intermixing width from Raman. The third, fifth, and sixth entries in the table correspond to the samples of Fig. 4.

The MBD sample exhibits the most diffraction orders (14), evidence of exceptional smoothness. We note that the interfacial width from Raman is always less than  $\xi$ .  $\xi$  and  $w$  were not measurements of precisely the same quantities. Here  $\xi$  contains a component from roughness and from intermixing, whereas Raman is an inherently interfacially sensitive technique for *a*-Si/*a*-Ge multilayers.

Having demonstrated the RS-interface technique, we applied it to study the influence of growth parameters on the interfacial sharpness in MBD multilayers. The first set of curves in Fig. 5 shows the Raman spectrum of a series of *a*-Si/*a*-Ge multilayers prepared at a fixed  $T_s = 300^\circ\text{C}$ . The period  $p$  has been varied from  $20\text{--}400\text{ \AA}$  and the nominal thickness of the individual layers was  $p/2$  for all cases. Broad Raman features characteristic of *a*-Si and *a*-Ge (Fig. 1) are observed in all multilayers with the exception of the one with  $p = 400\text{ \AA}$ . In the latter case, in addition to the amorphous com-

TABLE I. Properties<sup>a</sup> of various semiconductor multilayers.

Composition	Structure <sup>b</sup>	Technique <sup>c</sup>	$T_s$ (°C)	LAXRD <sup>d</sup>				Raman $w^e$
				$p^a$	$\xi^a$	$\eta$	$m$	
<i>a</i> -Si/ <i>a</i> -Ge	25 (50/50)	MBD	25					0.8
<i>a</i> -Si/ <i>a</i> -Ge	50 (10/10)	MBD	300	22				0.2
	25 (75/75)	MBD	300	154	4	0.54	14	1.0
	25 (100/100)	MBD	300					<0.5
<i>a</i> -Si/ <i>a</i> -Ge	25 (50/50)	IBS	275	104	7.8	0.53	9	3
<i>a</i> -Si/ <i>a</i> -Ge	100 (50/50)	MS	25	111	peak splitting		11	4
<i>a</i> -Si:H/ <i>a</i> -SiN:H	100 (20/20)	GD	250	54	5	0.6	4	not susceptible to analysis

<sup>a</sup> All thicknesses are in Angstroms.

<sup>b</sup> Number of periods (thickness of *a*-Si/thickness of *a*-Ge or SiN:H).

<sup>c</sup> MBD (molecular beam deposition), IBS (ion beam sputtering), MS (magnetron sputtering), and GD (glow discharge-plasma enhanced CVD).

<sup>d</sup> LAXRD data are  $p$  (periodicity),  $\xi$  (roughness),  $\eta$  ( $d_{Si}/p$  or  $d_{SiN}/p$ ),  $m$  (number of LAXRD peaks observed).

<sup>e</sup> Intermixing width,  $w = l_B - 2.2$ .

ponent, mainly silicon, there are two sharp lines located at approximately 300 and 520  $\text{cm}^{-1}$ . These indicate a totally microcrystalline germanium layer and a partially crystallized silicon layer, respectively. Notice that no significant interfacial mixing has occurred as indicated by the absence of the Si-Ge peak in the range of 380  $\text{cm}^{-1}$ .

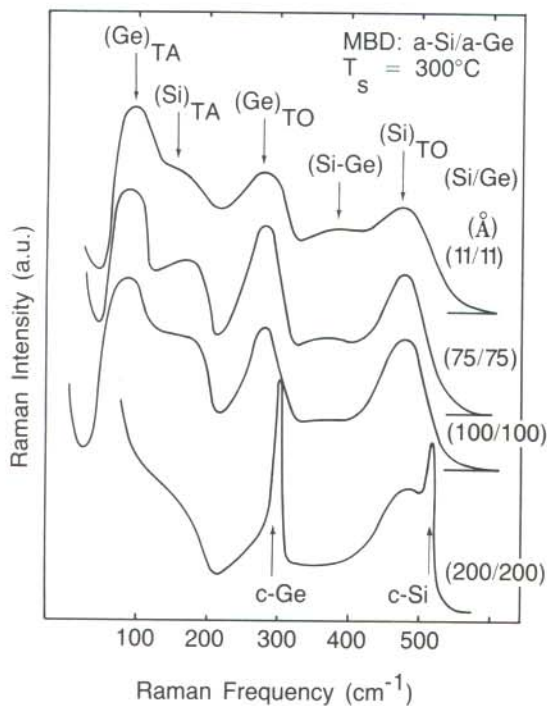


FIG. 5. Raman spectra for four Si/Ge multilayers prepared by MBD. Periodicities, top to bottom, are 22, 150, 200, and 400 Å, respectively. Nominal thicknesses for the Si and Ge layers in each sample are noted in a column on the left. All samples were prepared at a substrate temperature of  $T_s = 300^\circ\text{C}$ . The position of the Raman line for crystalline Ge and Si is indicated in the bottom of the figure.

The role that deposition temperature plays in achieving sharp interfaces from MBD multilayers was investigated. Samples prepared at 25  $^\circ\text{C}$  temperature exhibit a comparable Si-Ge peak equivalent to  $w = 0.8 \pm 0.2 \text{ \AA}$  vs  $1.0 \pm 0.2 \text{ \AA}$  for  $T_s = 300^\circ\text{C}$  (see Table I). There is no apparent increase in roughness due to decrease surface mobility of adatoms at lower  $T_s$ . It has been pointed out previously that the volume fractional voids in UHV *a*-Si and *a*-Ge decrease with increasing  $T_s$ . Above  $T_s = 200^\circ\text{C}$  (150  $^\circ\text{C}$ ) of *a*-Si (*a*-Ge), a thin film exhibits, via TEM, a void-free structure at a resolution of 50 Å. The absence of voids is evidence of higher adatom surface mobility that can dampen statistical variations in atomic flux and diminish self-shadowing effects.

Recent publications<sup>18</sup> have shown that Si and Ge prepared by ion beam sputtering using a Kaufman source exhibit a very dense structure. They suggest that the sputtered species impact the growing film with favorable energies that promote the densification of the material. Thus deposition at an elevated substrate temperature and high Ar beam voltage in an ion beam sputtering process might be a means of producing multilayer structures with sharp interfaces and regular periodicities.

A set of ion beam high vacuum (HV) sputtered multilayers have been prepared (see the IBS entry, Table I). The samples were positioned such that a large flux of elastically scatter Ar ions from the target reached the growing films surfaces, to provide densification. These ion beam sputtered *a*-Si/*a*-Ge multilayer films, however, exhibit a slightly wider  $w$  than the MBD samples; therefore, it appears that for the experimental conditions employed, the effect of ion beam induced mixing may be dominant over densification.

Several entries in Table I are conspicuously miss-

ing. These point to measurement difficulties characteristic of each technique. The RS does not lend itself to studying samples like GD *a*-Si:H/*a*-SiN:H. Since *a*-SiN:H is not strongly absorbing, there is not enough signal at the Raman wavelength. Furthermore, the interface is not characterized by a material like Si<sub>1-x</sub>Ge<sub>x</sub> that has distinct modes. On the other hand, the utility of LAXRD data is curtailed if the sample is not sufficiently uniform and regular like the MS sample. Raman spectroscopy does not have this limitation.

In the preceding analysis, for simplicity, it was assumed that the interfacial layer formed by deposited *a*-Ge on *a*-Si is the same as by *a*-Si deposited on *a*-Ge. If the adatom mobilities of the two are different, it can be expected that the interfaces will be different. This might show up in a shifting of the Si-Ge peak.

### ACKNOWLEDGMENTS

We acknowledge very helpful discussions with Dr. R. Tsu and Prof. F. H. Pollak. We would also like to thank E. M. Norman for her tenacity in preparing the manuscript.

Two of us, J. Gonzalez-Hernandez and D. Martin, acknowledge the support from The Standard Oil Company.

### REFERENCES

- <sup>1</sup>J. Kakalios, H. Fritzsche, N. Ibaraki, and S. R. Ovshinsky, *J. Non-Cryst. Solids* **66**, 339 (1984).
- <sup>2</sup>B. Abeles and T. Tiedje, *Phys. Rev. Lett.* **51**, 2003 (1983).
- <sup>3</sup>*Application of Thin Film Multilayer Structures to Figures X-Ray Optics*, SPIE Conference Proceedings, Vol. 563 (SPIE, Bellingham, WA, 1965), see, for example, p. 238; A. M. Kadin and J. E. Keem, *Scr. Metall.* **20**, 443 (1986).
- <sup>4</sup>J. H. Underwood and T. W. Barbee Jr., *AIP Conference Proceedings No. 75 on Low Energy X-Ray Diagnostics* (American Institute of Physics, New York, 1981), p. 170.
- <sup>5</sup>N. Maley and J. S. Lannin, *Phys. Rev. B* **31**, 5577 (1985).
- <sup>6</sup>P. D. Persans, A. F. Ruppert, B. Abeles, and T. Tiedje, *Phys. Rev. B* **32**, 5588 (1985).
- <sup>7</sup>J. Gonzales-Hernandez, D. D. Allred, O. V. Nguyen, D. Martin, and D. Pawlik, in *Layered Structures and Epitaxy*, edited by J. M. Gibson, G. C. Osbourn, and R. M. Tromp, Materials Research Society Symposium Proceedings, Vol. 56 (MRS, Pittsburgh, PA, 1986), pp. 389.
- <sup>8</sup>A. L. Greer and F. Spaepan, *Synthetic Modulated Structures*, edited by L. Chang and B. C. Giessen (Academic, New York, 1985), p. 419.
- <sup>9</sup>S. C. Agarwal and S. Guha, *Phys. Rev. B* **31**, 5547 (1985).
- <sup>10</sup>D. D. Allred and J. A. Piontkowski, in the *Proceedings of the Ninth International Conference on Chemical Vapor Deposition* (The Electrochemical Society, Pennington, NJ, 1984), p. 548.
- <sup>11</sup>R. Tsu, J. Gonzalez-Hernandez, J. Doehler, and S. R. Ovshinsky, *Solid State Commun.* **46**, 79 (1983).
- <sup>12</sup>R. Tsu, J. Gonzalez-Hernandez, S. S. Chao, S. C. Lee, and K. Tanaka, *Appl. Phys. Lett.* **40**, 534 (1982).
- <sup>13</sup>J. E. Smith Jr., M. H. Brodsky, B. L. Crowder, M. I. Nathan, and A. Pinczuk, *Phys. Rev. Lett.* **40**, 534 (1982).
- <sup>14</sup>F. Yndurian, *Phys. Rev. Lett.* **37**, 1062 (1976).
- <sup>15</sup>O. V. Nguyen, D. D. Allred, and J. Gonzales-Hernandez (unpublished).
- <sup>16</sup>S. S. Chao, J. Gonzalez-Hernandez, D. Martin, and R. Tsu, *Appl. Phys. Lett.* **46**, 1089 (1985).
- <sup>17</sup>R. Wolfe, *Applied Solid State Science* (Academic, New York, 1969), p. 210.
- <sup>18</sup>R. Collins, H. Windichmann, H. Cavese, and J. Gonzalez-Hernandez, *J. Appl. Phys.* **58**, 945 (1985).